

A measurement decoupling based fast algorithm for super-resolving point sources with multi-cluster structure

Ping Liu* and Hai Zhang[†]

April 4, 2022

Abstract

We consider the problem of resolving closely spaced point sources in one dimension from their Fourier data in a bounded domain. Classical subspace methods (e.g., MUSIC algorithm, Matrix Pencil method, etc.) show great superiority in resolving closely spaced sources, but their computational cost is usually heavy. This is especially the case for point sources with multi-cluster structure which requires processing large sized data matrix resulted from highly sampled measurement. To address this issue, we propose a fast algorithm termed D-MUSIC, based on a measurement decoupling strategy. We demonstrate theoretically that for point sources with a known cluster structure, their measurement can be decoupled into local measurements of each of the clusters by solving a system of linear equations that are obtained by using multipole basis. We further develop a subsampled MUSIC algorithm to detect the cluster structure and utilize it to decouple the global measurement. In the end, MUSIC algorithm was applied to each local measurement to resolve point sources therein. Compared to the standard MUSIC algorithm, the proposed algorithm has comparable super-resolving capability while having a much lower computational complexity.

1 Introduction

In recent years, with the rapid development of novel imaging techniques, super-resolution is drawing increasing interest in the fields of imaging, signal processing, and applied mathematics. In this paper, we consider the super-resolution problem of resolving closely spaced point sources in one dimension from their noisy Fourier data in a bounded domain. The goal is to develop an efficient algorithm for the case of point sources with multi-cluster structure defined below. See also Figure 1.1 for a typical example.

*Department of Mathematics, ETH Zürich, Swizerland (ping.liu@sam.math.ethz.ch).

[†]Department of Mathematics, HKUST, Clear Water Bay, Kowloon, Hong Kong, S.A.R, China (haizhang@ust.hk). Hai Zhang was partially supported by Hong Kong RGC grant GRF 16305419 and 16304621.

Definition 1.1. (*multi-cluster structure*)

Let Ω be a cutoff frequency and D be a constant of order one. Let Λ_j , $j = 1, 2, \dots, K$ be K intervals centered at O_j with half-length $\frac{D_j}{\Omega}$, respectively. We say that $\cup_{j=1}^K \Lambda_j$ is a (K, L, D, Ω) -region if

$$\max_{1 \leq j \leq K} D_j \leq D, \quad \min_{1 \leq i < j \leq K} |O_i - O_j| \geq \frac{L}{\Omega}.$$

We call that a set of point sources represented by a discrete measure μ has a multi-cluster structure if it is supported in a (K, L, D, Ω) -region with $D \ll L$.

Throughout the paper, we consider the following discrete measure with multi-cluster structure

$$\mu = \sum_{j=1}^K \sum_{q=1}^{n_j} a_{q,j} \delta_{y_{q,j}}, \quad (1.1)$$

where $y_{1,j}, \dots, y_{n_j,j}$ are the locations of point sources in Λ_j and $a_{1,j}, \dots, a_{n_j,j}$ their amplitudes. We denote

$$m_{\min,j} = \min_{q=1, \dots, n_j} |a_{q,j}|, \quad m = \|\mu\|_{TV} = \sum_{j=1}^K \sum_{q=1}^{n_j} |a_{q,j}|.$$

We assume that we have the Fourier transform of μ restricted to a bounded interval $[-\Omega, \Omega]$, where Ω is the cutoff frequency. We sample at N evenly-spaced points in the Fourier space to get the following discrete measurement

$$\mathbf{Y}(x_l) = \mathcal{F}[\mu](x_l) + \mathbf{W}(x_l) = \sum_{j=1}^K \mathbf{Y}_j(x_l) + \mathbf{W}(x_l), \quad x_l \in [-1, 1], \quad l = 1, \dots, N, \quad (1.2)$$

where

$$\mathbf{Y}_j(x_l) = \sum_{q=1}^{n_j} a_{q,j} e^{i y_{q,j} \Omega x_l}, \quad \mathcal{F}[\mu](x) := \int_{-\infty}^{\infty} \mu(y) e^{i \Omega y x} dy,$$

and $\mathbf{W}(x_l)$ is the additive noise. Throughout the paper, we call \mathbf{Y} the global measurement and \mathbf{Y}_j the local measurement generated by point sources in the cluster Λ_j . We write (1.2) into the following vector form

$$\mathbf{Y} = [\mu] + \mathbf{W} = \sum_{j=1}^K \mathbf{Y}_j + \mathbf{W} \quad (1.3)$$

where $\mathbf{Y} = (\mathbf{Y}(x_1), \dots, \mathbf{Y}(x_N))^T$, $[\mu] = (\mathcal{F}[\mu](x_1), \dots, \mathcal{F}[\mu](x_N))^T$, $\mathbf{W} = (\mathbf{W}(x_1), \dots, \mathbf{W}(x_N))^T$ and $\mathbf{Y}_j = (\mathbf{Y}_j(x_1), \dots, \mathbf{Y}_j(x_N))^T$. We assume

$$\frac{1}{\sqrt{N}} \|\mathbf{W}\|_2 \leq \sigma.$$

We are interested in the inverse problem of recovering the source locations $y_{1,1}, \dots, y_{n_K,K}$ from the measurement \mathbf{Y} . We note that by performing an inverse Fourier transform, the continuous measurement $\mathbf{Y}(x)$ is equivalent to the following spatial domain data

$$\hat{\mathbf{Y}}(t) = \sum_{j=1}^K \sum_{q=1}^{n_j} a_{q,j} \frac{\sin \Omega(t - y_{q,j})}{\pi t}.$$

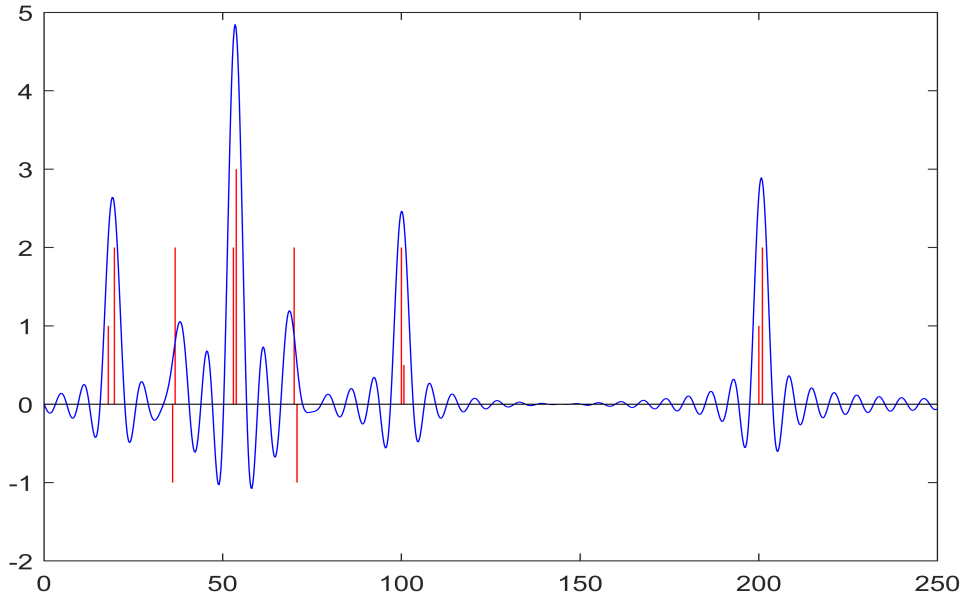


Figure 1.1: The blue curve represents spatial domain measurement; the red lines represent the to-be recovered point sources which are distributed in multiple clusters.

Then the inverse problem becomes a deconvolution problem in the spatial domain.

The inverse problem of (1.3) is severely ill-posed when there are multiple point sources closely spaced in one cluster, say with separation distance smaller than the Rayleigh length (RL) $\frac{\pi}{\Omega}$. For the case of a single cluster with closed spaced point sources, we refer the reader to [20–22] for a theory of computational resolution limit which addresses the theoretical issues of recovering source number and locations. We note that fine structures with scale smaller than RL cannot be resolved by the usual sparsity promoting optimization methods [3–9, 13, 23, 24, 29], which typically require a separation distance of several RLs (or some conditions to regularize the problem) [9, 28]. Alternatively one may consider the classical subspace methods (e.g., MUSIC [26], Matrix Pencil [16] and ESPRIT methods [25]), which have demonstrated super-resolving capacity [2, 17–19]. However, in the case of multiple clusters, highly sampled measurement is needed and this results large sized data matrix which demands high computational cost since these subspace algorithms rely on singular value decomposition.

To remedy these issues, we develop an efficient algorithm based on a measurement decoupling strategy. The main idea is that for a given measurement \mathbf{Y} that is generated by point sources as in (1.1) with a known cluster structure, one can first recover local measurement \mathbf{Y}_j for each j and then resolve sources in each cluster from their local measurement. We prove that when the clusters are well-separated, global measurement can be decomposed into local measurements by solving a system of linear equations that are obtained by using multipole basis. We further develop a subsampled MUSIC algorithm to detect the cluster structure and

utilize the result to decouple global measurement. A MUSIC algorithm was then applied to resolve point sources in each cluster from local measurement. It is demonstrated that the algorithm can super-resolve point sources when the clusters are well separated. Moreover, it has much lower computational complexity compared to standard MUSIC.

We notice that the idea of measurement decoupling was also exploited in [30]. Therein, the authors developed an algorithm for the two-dimensional DOA problem in array processing. They utilized a projection strategy to decouple the measurements of different groups in one dimension. Our measurement decoupling strategy is different. We use subsampled MUSIC algorithm to detect the cluster structure and then perform multipole expansion around each of the clustered centers. The local measurements are reconstructed using multipole basis.

On the other hand, if we assume that point sources are located on a grid, then the multi-cluster structure considered in this paper is related to block-sparse signals, see for instance [10–12, 27]. In [10, 27], the authors considered recovering \mathbf{X} from $\mathbf{Y} = \mathbf{DX}$, where

$$\mathbf{X} = \underbrace{(x_1, \dots, x_d)}_{\mathbf{x}^T[1]}, \underbrace{(x_{d+1}, \dots, x_{2d})}_{\mathbf{x}^T[2]}, \dots, \underbrace{(x_{N-d+1}, \dots, x_N)}_{\mathbf{x}^T[M]}^T$$

is a concatenation of M blocks of vectors of length D , and

$$\mathbf{D} = \underbrace{(\mathbf{D}_1, \dots, \mathbf{D}_d)}_{\mathbf{D}[1]}, \underbrace{(\mathbf{D}_{d+1}, \dots, \mathbf{D}_{2d})}_{\mathbf{D}[2]}, \dots, \underbrace{(\mathbf{D}_{N-d+1}, \dots, \mathbf{D}_N)}_{\mathbf{D}[M]}$$

is a concatenation of M blocks of matrices of size $L \times d$. The authors proposed the following relaxation scheme to reconstruct \mathbf{X} [27]:

$$\min \sum_{l=1}^M \|\mathbf{X}[l]\|_2, \text{ subject to } \mathbf{DX} = \mathbf{Y}. \quad (1.4)$$

They demonstrated that when the block matrices $\mathbf{D}[j]$'s are Gaussian, (1.4) can find the sparsest solution \mathbf{X} with overwhelming probability as $N \rightarrow \infty$ under certain conditions. In [11], based on block-coherence measure, the authors showed that any block k -sparse vector can be recovered if the block-coherence satisfies certain condition. However, this condition does not hold for the measurement matrix when resolving closely spaced point sources as is considered in this paper.

The rest of the paper is organized in the following way. In Section 2, we introduce the theory and strategy for measurement decoupling. In Section 3, we develop a subsampled MUSIC algorithm to detect cluster structures. In Section 4, we develop the measurement decoupling based algorithm, D-MUSIC, for resolving point sources with multi-cluster structure. We also conduct numerical experiments to demonstrate its efficiency. Finally, in Section 5, we outline some future works.

2 The theory of measurement decoupling by using multipole basis

In this section, we develop the theory of measurement decoupling using multipole basis. The aim is to decouple local measurements \mathbf{Y}_j 's from the global measurement \mathbf{Y} in (1.2) for point

sources (1.1) with a known multi-cluster structure. The main idea is to first represent each of the local measurement \mathbf{Y}_j using a proper set of multipole basis, and then decouple them by solving a system of linear equations. We show that the strategy works when the clusters are well-separated. In section 2.1, we develop the theory using multipole basis in a straightforward manner. In section 2.2, we improve the decoupling strategy by using a modulation technique.

2.1 Decoupling using multipole basis—a precursor

We start with the following multipole expansion for the local measurement \mathbf{Y}_j ,

$$\begin{aligned} \mathbf{Y}_j(x) &= \sum_{q=1}^{n_j} a_{q,j} e^{i\Omega y_{q,j} x} = \sum_{q=1}^{n_j} a_{q,j} e^{i\Omega O_j x} e^{i\Omega(y_{q,j}-O_j)x} \\ &= \sum_{q=1}^{n_j} a_{q,j} \sum_{r=0}^{\infty} e^{i\Omega O_j x} \frac{(i\Omega(y_{q,j}-O_j)x)^r}{r!} \\ &= \sum_{r=0}^{\infty} \sum_{q=1}^{n_j} a_{q,j} (\Omega(y_{q,j}-O_j))^r e^{i\Omega O_j x} \frac{(ix)^r}{r!}. \end{aligned} \quad (2.1)$$

We call the function $h_{r,O_j}(x) = \sqrt{2r+1} e^{i\Omega O_j x} (ix)^r$ the r -th order multipole function centered at O_j . Let x_1, x_2, \dots, x_N be N equally spaced sample point in $[-1, 1]$. We define its discretized version by

$$\mathbf{h}_{r,O_j} = (h_{r,O_j}(x_1), \dots, h_{r,O_j}(x_N))^T, \quad (2.2)$$

and call it the r -th order multipole basis vector centered at O_j . We have

$$\frac{1}{\sqrt{N}} \|\mathbf{h}_{r,O_j}\|_2 \approx \sqrt{\frac{1}{2} \int_{-1}^1 (2r+1)x^{2r} dx} \leq 1, \quad 1 \leq j \leq K, r = 0, 1, \dots \quad (2.3)$$

We define

$$Q_{r,O_j}(\mu) = \frac{\sum_{q=1}^{n_j} a_{q,j} (\Omega(y_{q,j}-O_j))^r}{\sqrt{2r+1} r!} \quad (2.4)$$

and call it multipole coefficient. Using multiple basis vectors, we have the following representation for the global measurement \mathbf{Y} :

$$\mathbf{Y} = \sum_{j=1}^K \sum_{r=0}^{\infty} Q_{r,O_j} \mathbf{h}_{r,O_j} + \mathbf{W}. \quad (2.5)$$

Observing that higher order multipole basis vectors decay exponentially fast as the order increases, we thus can approximate \mathbf{Y} by the first s multipole basis vectors in each of the clusters, where s is to be determined. For the purpose, denote

$$\mathbf{H}[j] = (\mathbf{h}_{0,O_j}, \dots, \mathbf{h}_{s-1,O_j}) \quad (2.6)$$

by the multipole matrix associated with the cluster centered at O_j , and

$$\boldsymbol{\theta}_j = (Q_{0,O_j}, \dots, Q_{s-1,O_j})$$

by the vector of multipole coefficients. We have

$$\mathbf{Y} = \sum_{j=1}^K \mathbf{H}[j] \boldsymbol{\theta}_j + \mathbf{W} + \mathbf{Res}, \quad (2.7)$$

where \mathbf{Res} is the residual term. Now, we determine s . For a given σ , m , and D , we choose

$$s := \min \left\{ l \in \mathbb{N} : \frac{D^l(l+1)}{l! \sqrt{2l+1}(l+1-D)} \leq \frac{\sigma}{m}, l \geq D \right\}. \quad (2.8)$$

Then

$$\begin{aligned} \frac{1}{\sqrt{N}} \|\mathbf{Res}\|_2 &= \frac{1}{\sqrt{N}} \left\| \sum_{r=s}^{+\infty} \sum_{j=1}^K \sum_{q=1}^{n_j} \frac{a_{q,j} (\Omega(y_{q,j} - O_j))^r}{r! \sqrt{2r+1}} \mathbf{h}_{r,O_j} \right\|_2 \\ &\leq \sum_{r=s}^{+\infty} \sum_{j=1}^K \sum_{q=1}^{n_j} \frac{|a_{q,j}| |\Omega(y_{q,j} - O_j)|^r}{r! \sqrt{2r+1}} \frac{1}{\sqrt{N}} \|\mathbf{h}_{r,O_j}\|_2 \lesssim m \sum_{r=s}^{+\infty} \frac{D^r}{r! \sqrt{2r+1}} \quad (\text{by (2.3)}) \\ &= m \frac{D^s}{s! \sqrt{2s+1}} \left(1 + \frac{D}{s+1} + \frac{D^2}{(s+1)(s+2)} + \dots \right) \\ &< m \frac{D^s}{s! \sqrt{2s+1}} \frac{1}{1 - \frac{D}{s+1}} = m \frac{D^s(s+1)}{s! \sqrt{2s+1}(s+1-D)} \leq \sigma. \quad (\text{by (2.8)}) \end{aligned} \quad (2.9)$$

Therefore, \mathbf{Res} is of noise level with s chosen above.

We next present a result on the correlation between vectors spanned by multipole basis vectors associated with different clusters.

Lemma 2.1. *Let $\mathbf{H}[j], \mathbf{H}[p]$ be defined as in (2.6). Assume that $|O_j - O_p| \geq \frac{2(2s-2)^2}{\Omega}$, then*

$$\lim_{N \rightarrow \infty} \left| \left\langle \frac{1}{\sqrt{N}} \mathbf{H}[j] \mathbf{a}_j, \frac{1}{\sqrt{N}} \mathbf{H}[p] \mathbf{a}_p \right\rangle \right| < \frac{3.2(2s-1)^2}{|\Omega(O_j - O_p)|} \lim_{N \rightarrow \infty} \left\| \frac{1}{\sqrt{N}} \mathbf{H}[j] \mathbf{a}_j \right\|_2 \left\| \frac{1}{\sqrt{N}} \mathbf{H}[p] \mathbf{a}_p \right\|_2.$$

Proof. Note that

$$\begin{aligned} &\lim_{N \rightarrow \infty} \left| \left\langle \frac{1}{\sqrt{N}} \mathbf{H}[j] \mathbf{a}_j, \frac{1}{\sqrt{N}} \mathbf{H}[p] \mathbf{a}_p \right\rangle \right| \\ &= \left| \int_{-1}^1 e^{i\Omega(O_j - O_p)x} \sum_{q_1, q_2=0}^{s-1} a_{q_1,j} \bar{a}_{q_2,p} i^{q_1} (-i)^{q_2} \sqrt{2q_1+1} \sqrt{2q_2+1} x^{q_1+q_2} dx \right|. \end{aligned}$$

Let $\psi(x) = \sum_{q_1, q_2=0}^{s-1} a_{q_1,j} \bar{a}_{q_2,p} i^{q_1} (-i)^{q_2} \sqrt{2q_1+1} \sqrt{2q_2+1} x^{q_1+q_2}$. By Lemmas 6.3 and 6.2 we have

$$\left| \int_{-1}^1 e^{i\Omega(O_j - O_p)x} \psi(x) dx \right| < \frac{3.2 \|\psi\|_{L^\infty([-1,1])}}{|\Omega(O_j - O_p)|} \leq \frac{3.2(2s-1)^2 \|\psi\|_{L_1([-1,1])}}{|\Omega(O_j - O_p)|}.$$

Finally, by Cauchy–Schwarz inequality we have

$$\begin{aligned} \|\psi\|_{L_1([-1,1])} &\leq \sqrt{\int_{-1}^1 \left| \sum_{q_1=0}^{s-1} a_{q_1,j} \sqrt{2q_1+1} x^{q_1} \right|^2 dx} \sqrt{\int_{-1}^1 \left| \sum_{q_2=0}^{s-1} a_{q_2,p} \sqrt{2q_2+1} x^{q_2} \right|^2 dx} \\ &= \lim_{N \rightarrow \infty} \left\| \frac{1}{\sqrt{N}} \mathbf{H}[j] \mathbf{a}_j \right\|_2 \left\| \frac{1}{\sqrt{N}} \mathbf{H}[p] \mathbf{a}_p \right\|_2. \end{aligned}$$

This completes the proof. \square

Remark 2.1. *Lemmas 2.1 demonstrates that when the clusters are well separated, the spaces spanned by multipole basis vectors associated with different clusters are nearly orthogonal to each other. In comparison, we note that in a recent paper [1], the authors obtained similar result for the column vectors of Vandermonde matrix.*

We are ready to present a first result on the decoupling theory.

Proposition 2.1. *Suppose N is large enough and that the point sources in (1.1) is supported in a (K, L, D, Ω) -region. Suppose*

$$L \geq 12.8(2s-1)^2 \left(\ln\left(\frac{K}{2}\right) + 1 \right) \quad (2.10)$$

with s being defined by (2.8). Let

$$(\mathbf{a}_1, \dots, \mathbf{a}_K) = \operatorname{argmin}_{\boldsymbol{\theta}_j} \frac{1}{\sqrt{N}} \left\| \sum_{j=1}^K \mathbf{H}[j] \boldsymbol{\theta}_j - \mathbf{Y} \right\|_2, \quad (2.11)$$

then we have

$$\frac{1}{\sqrt{N}} \left\| \mathbf{H}[j] \mathbf{a}_j - \mathbf{Y}_j \right\|_2 \lesssim \sigma, \quad 1 \leq j \leq K,$$

where \mathbf{Y}_j 's are the local measurements in (1.3).

Proof. Note that

$$\frac{1}{\sqrt{N}} \left\| \sum_{j=1}^K \mathbf{Y}_j - \mathbf{Y} \right\|_2 \leq \sigma. \quad (2.12)$$

For each local measurement \mathbf{Y}_j , similar to (2.20), we have

$$\mathbf{Y}_j = \mathbf{H}[j] \mathbf{b}_j + \mathbf{Res}_j, \quad (2.13)$$

where $\mathbf{b}_j = (Q_{0,O_j}, \dots, Q_{s-1,O_j})^T$ with $Q_{r,O_j} = \sum_{q=1}^{n_j} \frac{a_{q,j} (\Omega(y_{q,j} - O_j))^r}{r! \sqrt{2r+1}}$, and \mathbf{Res}_j is the residual term.

Similar to (2.9), we have $\frac{1}{\sqrt{N}} \left\| \sum_{j=1}^K \mathbf{Res}_j \right\|_2 \lesssim \sigma$. Together with (2.12), it follows that

$\frac{1}{\sqrt{N}} \left\| \sum_{j=1}^K \mathbf{H}[j] \mathbf{b}_j - \mathbf{Y} \right\|_2 \lesssim \sigma$. On the other hand, it is clear that $\frac{1}{\sqrt{N}} \left\| \sum_{j=1}^K \mathbf{H}[j] \mathbf{a}_j - \mathbf{Y} \right\|_2 \lesssim \sigma$. Therefore

$$\frac{1}{\sqrt{N}} \left\| \sum_{j=1}^K \mathbf{H}[j] (\mathbf{a}_j - \mathbf{b}_j) \right\|_2 \lesssim \sigma. \quad (2.14)$$

We next estimate the approximation of the local measurements. Consider $\frac{1}{\sqrt{N}} \left\| \mathbf{H}[j] (\mathbf{a}_j - \right.$

$\mathbf{b}_j\|_2, 1 \leq j \leq K$ at first. Let $\mathbf{v}_j = \frac{1}{\sqrt{N}}\mathbf{H}[j](\mathbf{a}_j - \mathbf{b}_j)$, for large enough N , we have

$$\begin{aligned}
& \frac{1}{N} \left\| \sum_{j=1}^K \mathbf{H}[j](\mathbf{a}_j - \mathbf{b}_j) \right\|_2^2 = \left\| \sum_{j=1}^K \mathbf{v}_j \right\|_2^2 = \sum_{j=1}^K \left\| \mathbf{v}_j \right\|_2^2 + \sum_{j=1}^K \sum_{p \neq j} \langle \mathbf{v}_j, \mathbf{v}_p \rangle \\
& \geq \sum_{j=1}^K \left\| \mathbf{v}_j \right\|_2^2 - \sum_{j=1}^K \sum_{p \neq j} \frac{3.2(2s-1)^2}{|\Omega(O_j - O_p)|} \left\| \mathbf{v}_j \right\|_2 \left\| \mathbf{v}_p \right\|_2 \quad (\text{by Lemma 2.1}) \\
& \geq \sum_{j=1}^K \left\| \mathbf{v}_j \right\|_2^2 - \sum_{j=1}^K \sum_{p \neq j} \frac{1.6(2s-1)^2}{|\Omega(O_j - O_p)|} \left(\left\| \mathbf{v}_j \right\|_2^2 + \left\| \mathbf{v}_p \right\|_2^2 \right) \\
& \geq \sum_{j=1}^K \left(\left\| \mathbf{v}_j \right\|_2^2 - \sum_{p \neq j} \frac{3.2(2s-1)^2}{|\Omega(O_j - O_p)|} \left\| \mathbf{v}_j \right\|_2^2 \right) \\
& \geq \frac{1}{2} \sum_{j=1}^K \left\| \mathbf{v}_j \right\|_2^2 = \sum_{j=1}^K \frac{1}{2N} \left\| \mathbf{H}[j](\mathbf{a}_j - \mathbf{b}_j) \right\|_2^2,
\end{aligned} \tag{2.15}$$

where the last inequality is derived from the assumption (2.10) and the inequality $\sum_{p=1, p \neq j}^K \frac{1}{|p-j|} < 2(\ln \frac{K}{2} + 1)$. Using (2.14), it follows that

$$\frac{1}{\sqrt{N}} \left\| \mathbf{H}[j](\mathbf{a}_j - \mathbf{b}_j) \right\|_2 \lesssim \sigma, \quad j = 1, \dots, K.$$

Furthermore, by (2.13) and $\frac{1}{\sqrt{N}} \|\mathbf{Res}_j\|_2 \lesssim \sigma$, we have

$$\frac{1}{\sqrt{N}} \left\| \mathbf{H}[j]\mathbf{a}_j - \mathbf{Y}_j \right\|_2 \lesssim \sigma, \quad j = 1, \dots, K,$$

which completes the proof. \square

We observe that in Proposition 2.1 the minimum separation distance between clusters depends on the number of the clusters K . This is due to the slow decay of the correlation between vectors in the span of multipole basis vectors associated with different clusters with respect to the cluster separation distance (see Lemma 2.1). To remedy this issue, we employ a modulation technique. This is done in the next section.

2.2 Measurement decoupling using multipole basis with modulation

In this section, we decouple global measurement using modulated multipole basis. The modulation is intended to reduce the correlation between the multipole basis vectors from different clusters. For ease of presentation, we consider the following modulation function throughout

$$f^t(x) = 1 - x^2, \quad x \in [-1, 1].$$

Other smooth functions with support in $[-1, 1]$ can be used as a modulation function as well and the treatment is similar. Throughout the paper, the superscript t indicates that quantity is associated with modulation. We define

$$h_{r, O_j}^t(x) = \sqrt{2r+1} e^{i\Omega_j x} (ix)^r f^t(x)$$

to be the r -th order modulated multipole function centered at O_j and

$$\mathbf{h}_{r,O_j}^t = (h_{r,O_j}^t(x_1), \dots, h_{r,O_j}^t(x_N))^T \quad (2.16)$$

its discretized version. We similarly have

$$\frac{1}{\sqrt{N}} \|\mathbf{h}_{r,O_j}^t\|_2 \lesssim 1, \quad 1 \leq j \leq K, r = 0, 1, \dots.$$

We consider the modulated measurement

$$\mathbf{Y}^t(x_l) = f^t(x_l) \mathcal{F}[\mu](x_l) + f^t(x_l) \mathbf{W}(x_l) = \sum_{j=1}^K \mathbf{Y}_j^t(x_l) + \mathbf{W}^t(x_l), \quad x_l \in [-1, 1], l = 1, \dots, N. \quad (2.17)$$

Or equivalently

$$\mathbf{Y}^t = \sum_{j=1}^K \sum_{r=0}^{\infty} Q_{r,O_j} \mathbf{h}_{r,O_j}^t + \mathbf{W}^t, \quad (2.18)$$

where Q_{r,O_j} is the same as defined in (2.4). Define s as in (2.8), and

$$\mathbf{H}^t[j] = (\mathbf{h}_{0,O_j}^t, \dots, \mathbf{h}_{s-1,O_j}^t), \quad \boldsymbol{\theta}_j = (Q_{0,O_j}, \dots, Q_{s-1,O_j})^T. \quad (2.19)$$

We have

$$\mathbf{Y}^t = \sum_{j=1}^K \mathbf{H}^t[j] \boldsymbol{\theta}_j + \mathbf{W}^t + \mathbf{Res}^t. \quad (2.20)$$

We can also show that $\frac{1}{\sqrt{N}} \|\mathbf{Res}^t\|_2 \lesssim \sigma$. Therefore, $\sum_{j=1}^K \mathbf{H}^t[j] \boldsymbol{\theta}_j$ can approximate \mathbf{Y}^t to the noise level.

We next show that the decay of the correlation between vectors in the span of modulated multipole basis vectors associated with different clusters with respect to the cluster separation distance is indeed enhanced, in comparison to Lemma 2.1.

Lemma 2.2. For $\mathbf{H}^t[j], \mathbf{H}^t[p], p \neq j$ defined as in (2.19), assume that $|O_j - O_p| \geq \frac{2(2s+2)^2}{\Omega}$. Then

$$\begin{aligned} & \lim_{N \rightarrow \infty} \left| \left\langle \frac{1}{\sqrt{N}} \mathbf{H}^t[j] \mathbf{a}_j, \frac{1}{\sqrt{N}} \mathbf{H}^t[p] \mathbf{a}_p \right\rangle \right| \\ & < \frac{0.8(2s+2)^4(2s+3)^2}{|\Omega(O_j - O_p)|^3} \lim_{N \rightarrow \infty} \left\| \frac{1}{\sqrt{N}} \mathbf{H}^t[j] \mathbf{a}_j \right\|_2 \left\| \frac{1}{\sqrt{N}} \mathbf{H}^t[p] \mathbf{a}_p \right\|_2. \end{aligned}$$

Proof. The proof is similar to that of Lemma 2.2. It utilizes the second estimate in Lemma 6.3 since $f(\pm 1) = 0, f'(\pm 1) = 0$ for $f(x) = 1 - x^2$. \square

We have the following main result on the measurement decoupling using multipole basis with modulation.

Theorem 2.1. Suppose N is large enough and the point sources in (1.1) is supported in a (K, L, D, Ω) -region. Suppose

$$L \geq 4^{1/3}(2s+3)^2 \quad (2.21)$$

with s being defined by (2.8). Let

$$(\mathbf{a}_1, \dots, \mathbf{a}_K) = \arg \min_{\boldsymbol{\theta}_j} \frac{1}{\sqrt{N}} \left\| \sum_{j=1}^K \mathbf{H}^t[j] \boldsymbol{\theta}_j - \mathbf{Y}^t \right\|_2. \quad (2.22)$$

We have

$$\frac{1}{\sqrt{N}} \left\| \mathbf{H}^t[j] \mathbf{a}_j - \mathbf{Y}_j^t \right\|_2 \lesssim \sigma \quad (2.23)$$

for each local measurement $\mathbf{Y}_j^t, 1 \leq j \leq K$ in (2.17).

Proof. In the same fashion as the proof of Proposition 2.1, for multipole expansion

$$\mathbf{Y}_j^t = \mathbf{H}^t[j] \mathbf{b}_j + \mathbf{Res}_j^t,$$

we can show that

$$\frac{1}{\sqrt{N}} \left\| \sum_{j=1}^K \mathbf{H}^t[j] (\mathbf{a}_j - \mathbf{b}_j) \right\|_2 \lesssim \sigma. \quad (2.24)$$

Let $\mathbf{v}_j = \frac{1}{\sqrt{N}} \mathbf{H}^t[j] (\mathbf{a}_j - \mathbf{b}_j)$, for large enough N , we have

$$\begin{aligned} & \frac{1}{N} \left\| \sum_{j=1}^K \mathbf{H}^t[j] (\mathbf{a}_j - \mathbf{b}_j) \right\|_2^2 = \left\| \sum_{j=1}^K \mathbf{v}_j \right\|_2^2 = \sum_{j=1}^K \left\| \mathbf{v}_j \right\|_2^2 + \sum_{j=1}^K \sum_{p \neq j} \langle \mathbf{v}_j, \mathbf{v}_p \rangle \\ & \geq \sum_{j=1}^K \left\| \mathbf{v}_j \right\|_2^2 - \sum_{j=1}^K \sum_{p \neq j} \frac{0.8(2s+2)^4(2s+3)^2}{|\Omega(O_j - O_p)|^3} \left\| \mathbf{v}_j \right\|_2 \left\| \mathbf{v}_p \right\|_2 \\ & \geq \sum_{j=1}^K \left\| \mathbf{v}_j \right\|_2^2 - \sum_{j=1}^K \sum_{p \neq j} \frac{0.4(2s+2)^4(2s+3)^2}{|\Omega(O_j - O_p)|^3} \left(\left\| \mathbf{v}_j \right\|_2^2 + \left\| \mathbf{v}_p \right\|_2^2 \right) \\ & \geq \sum_{j=1}^K \left(\left\| \mathbf{v}_j \right\|_2^2 - \sum_{p \neq j} \frac{0.8(2s+2)^4(2s+3)^2}{|\Omega(O_j - O_p)|^3} \left\| \mathbf{v}_j \right\|_2^2 \right) \\ & \geq \frac{1}{2} \sum_{j=1}^K \left\| \mathbf{v}_j \right\|_2^2 = \sum_{j=1}^K \frac{1}{2N} \left\| \mathbf{H}^t[j] (\mathbf{a}_j - \mathbf{b}_j) \right\|_2^2, \end{aligned} \quad (2.25)$$

where the last inequality follows from (2.21) and the estimate that $\sum_{p=1, p \neq j}^K \frac{1}{|p-j|^3} < 2.5$. Using (2.24), we get

$$\frac{1}{\sqrt{N}} \left\| \mathbf{H}^t[j] (\mathbf{a}_j - \mathbf{b}_j) \right\|_2 \lesssim \sigma, \quad j = 1, \dots, K.$$

Therefore

$$\frac{1}{\sqrt{N}} \left\| \mathbf{H}^t[j] \mathbf{a}_j - \mathbf{Y}_j^t \right\|_2 \lesssim \sigma, \quad j = 1, \dots, K,$$

which completes the proof. \square

Theorem 2.1 demonstrates that the global modulated measurement can be decoupled into local modulated measurements when the clusters are well-separated. Compared to Proposition 2.1, the required separation distance between clusters is reduced due to the modulation technique. There is an alternative explanation to this. Observe that the point spread function (the measurement data in the spatial domain corresponding to a single point source) corresponding to the modulated measurement is given by

$$\int_{-1}^1 (1-x^2)e^{-itx} dx.$$

By Lemma 6.3, it has a decay rate of $1/|t^3|$, which is faster than the un-modulated one which has a decay rate of $1/|t|$. Therefore, the local modulated measurements associated with different clusters are more decorrelated as their separation distance increases.

On the other hand, we note that local measurements can be reconstructed by dividing the modulated ones $\mathbf{H}^t[j]\mathbf{a}_j$'s point-wisely by the modulation function f^t . Note that $f^t \approx 0$ for $x \approx \pm 1$. Therefore, only frequency components that are away from ± 1 can be reconstructed stably, and those near the end points have to be discarded from the modulation technique. It can be shown that by choosing modulation function f^t that has higher order of degeneracy at the end points ± 1 , one can improve the performance, both theoretically and numerically, of the decoupling of global modulated measurement. However, the benefit is at the cost of losing frequency component near the end points in the recovered local measurements. It is an interesting and important question to choose the optimal modulation function in practice. We leave this for a future investigation.

Remark 2.2. *Sufficiently many multipole basis vectors are needed for the measurement decoupling strategy in the above theorem. The choice of s satisfying (2.8) cannot be improved. Numerical experiments show that when the number of required multipole basis vectors s is not big enough, local measurements cannot be recovered successfully from (2.22) even though the clusters are well-separated and the global measurement is approximated to noise level.*

Finally, we note that in Proposition 2.1 and Theorem 2.1, the lower bound of L depends on s in a quadratic manner. However, this estimate may not be optimal. On the other hand, it is clear that the lower bound increases as s increases. In the next section, we conduct numerical experiments to demonstrate this dependence relation.

2.3 The minimum required L for the measurement decoupling

In this section, we numerically investigate the dependence of the minimum required separation distance between clusters L on the multipole number s for the two decoupling strategies in section 2.1 and 2.2. It is demonstrated that the modulation technique can relax the condition on the separation distance between clusters.

We first consider the decoupling strategy using the modulation technique in section 2.2. For simplicity, we set $\Omega = 1$, $m = 1$, $\sigma = 10^{-3}$, and the number of samples $N = 1000$. We investigate the minimum L required for $s = 3, \dots, 29$, separately. More precisely, for each $s \in \{3, \dots, 29\}$, we construct several D 's satisfying (2.8) with $\sigma = 10^{-3}$, and perform at least 1000 random experiments for each pair (D, L) with $L \in \{3\pi, 3.5\pi, 4\pi, \dots, 50\pi\}$ being the lower bound for cluster

separation distance. We consider realizations of point sources in a $(K, L, D, \Omega = 1)$ -region with cluster number K and cluster centers chosen randomly. We decouple the measurement as in Theorem 2.1. We then construct the multipole basis $\mathbf{H}^t[j]$'s and approximate the global measurement \mathbf{Y}^t . The global measurement is considered being well approximated if

$$\frac{1}{\sqrt{N}} \left\| \sum_{j=1}^K \mathbf{H}^t[j] \hat{\mathbf{a}}_j - \mathbf{Y}^t \right\|_2 \leq 3\sigma. \quad (2.26)$$

If this is the case, we further recover the multipole coefficients by using (2.22) and construct the local measurements. The measurement decoupling is regarded as successful if $\frac{1}{\sqrt{N}} \|\mathbf{H}^t[j] \hat{\mathbf{a}}_j - \mathbf{Y}_j^t\|_2 < 6\sigma$ for all j , and otherwise unsuccessful.

We view that the measurement decoupling strategy is successful for point sources with multi-cluster structure determined by the pair (D, L) if the success ratio out of 1000 random experiments is greater than 99%. For each $s \in \{3, \dots, 29\}$, we denote $L(s)$ as the minimum L in all the corresponding pairs (D, L) 's for successful measurement decoupling. We summarize the relation of s and the $L(s)$ in Tables 2.1. We perform similar experiments to the decoupling strategy in section 2.1. To compare the two decoupling strategy, we plot the relation of required minimum separation distance of clusters with respect to the multipole number s for both strategies in Figure 2.1. It is shown that the technique of modulation can indeed relax the minimum required separation distance of clusters for stable measurement decoupling.

s	3	4	5	6	7	8	9	10	11
L(s)	3π	4π	5π	6π	7π	8π	9π	10π	11π
s	12	13	14	15	16	17	18	19	20
L(s)	12π	13π	14π	15π	16π	18π	19.5π	21π	22.5π
s	21	22	23	24	25	26	27	28	29
L(s)	24π	26π	27.5π	29.5π	31.5π	33π	36.5π	38.5π	40.5π

Table 2.1: Minimum separation of clusters for stably decoupling modulated measurements

3 A subsampled MUSIC algorithm for cluster structure detection

In this section, we develop a subsampled MUSIC algorithm to detect cluster structure for a given set of point sources with multi-cluster structure.

3.1 MUSIC algorithm

We first review the standard MUSIC algorithm. We then incorporate a prior information on the cluster structure of point sources to make it more efficient. For simplicity, we set $\Omega = 1$ in the subsequent presentation.

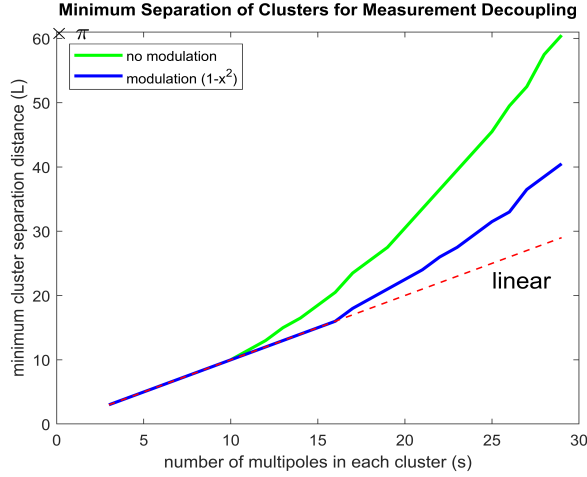


Figure 2.1: Plot of the minimum separation of clusters for measurement decoupling. It is shown that the required minimum separation distance between clusters can be relaxed by measurement modulation.

In a standard MUSIC algorithm for solving the inverse problem (1.2), one first assemble the following Hankel matrix

$$\hat{X} = \begin{pmatrix} \mathbf{Y}(x_1) & \mathbf{Y}(x_2) & \cdots & \mathbf{Y}(x_{\hat{N}}) \\ \mathbf{Y}(x_2) & \mathbf{Y}(x_3) & \cdots & \mathbf{Y}(x_{\hat{N}+1}) \\ \cdots & \cdots & \ddots & \cdots \\ \mathbf{Y}(x_{\hat{N}}) & \mathbf{Y}(x_{\hat{N}+1}) & \cdots & \mathbf{Y}(x_{2\hat{N}+1}) \end{pmatrix}, \quad (3.1)$$

where $\hat{N} = \lfloor \frac{N-1}{2} \rfloor$. Then perform singular value decomposition for \hat{X} ,

$$\hat{X} = \hat{U} \hat{\Sigma} \hat{U}^* = [\hat{U}_1 \quad \hat{U}_2] \text{diag}(\hat{\sigma}_1, \hat{\sigma}_2, \dots, \hat{\sigma}_n, \hat{\sigma}_{n+1}, \dots, \hat{\sigma}_{\hat{N}+1}) [\hat{U}_1 \quad \hat{U}_2]^*,$$

where $\hat{U}_1 = (\hat{U}(1), \dots, \hat{U}(n))$, $\hat{U}_2 = (\hat{U}(n+1), \dots, \hat{U}(\hat{N}+1))$ with n being the estimated source number (model order). The source number n can be detected by many algorithms such as those in [14, 15, 21, 31]. Denote the orthogonal projection to the space \hat{U}_2 by $\hat{P}_2 x = \hat{U}_2 (\hat{U}_2^* x)$. For a test vector $\Phi(\omega) = (1, e^{ih\omega}, \dots, e^{i\hat{N}h\omega})^T$ with h being the spacing parameter, one define the MUSIC imaging functional

$$\hat{J}(\omega) = \frac{\|\Phi(\omega)\|_2}{\|\hat{P}_2 \Phi(\omega)\|_2} = \frac{\|\Phi(\omega)\|_2}{\|\hat{U}_2^* \Phi(\omega)\|_2}.$$

The local maximizers of $\hat{J}(\omega)$ indicate the locations of the point sources. In practice, one can test evenly spaced points in a specified region and plot the discrete imaging functional and then determine the source locations by detecting the peaks. A peak selection algorithm is

given in the appendix. We summarize the standard MUSIC algorithm in **Algorithm 1** below.

Algorithm 1: Standard MUSIC algorithm

- Input:** Noise level σ , Measurements: $\mathbf{Y} = (\mathbf{Y}(x_1), \dots, \mathbf{Y}(x_N))^T$ with h the sampling distance;
- Input:** Region of test points $[TS, TE]$ and spacing of test points TPS ;
- 1: Let n be the estimated source number;
- 2: Let $\hat{N} = \lfloor \frac{N-1}{2} \rfloor$, formulate the $(\hat{N} + 1) \times (\hat{N} + 1)$ Hankel matrix \hat{X} from \mathbf{Y} ;
- 3: Compute the singular vector of \hat{X} as $\hat{U}(1), \hat{U}(2), \dots, \hat{U}(\hat{N} + 1)$ and formulate the noise space $\hat{U}_2 = (\hat{U}(n + 1), \dots, \hat{U}(\hat{N} + 1))$;
- 4: For test points ω 's in $[TS, TE]$ evenly spaced by TPS , construct the test vector $\Phi(\omega) = (1, e^{ih\omega}, \dots, e^{i\hat{N}h\omega})^T$;
- 5: Plot the MUSIC imaging functional $\hat{J}(\omega) = \frac{\|\Phi(\omega)\|_2}{\|\hat{U}_2^* \Phi(\omega)\|_2}$;
- 6: Select the peak locations \hat{y}_j 's in the $\hat{J}(\omega)$ by **Algorithm 6**;
- Return** \hat{y}_j 's.
-

Now, assume that the point sources we are interested in are located in an interval $\Lambda = [O - D, O + D]$ that centered at O with size D . We can incorporate this a prior information into the standard MUSIC to make it more efficient. To be more specific, let y_1, \dots, y_n be the point sources and its measurement without noise is given by

$$\mathbf{Y}(x_l) = \sum_{q=1}^n a_q e^{iy_q x_l}, \quad x_l \in [-1, 1], \quad q = 1, \dots, n. \quad (3.2)$$

Observe that

$$\mathbf{Y}(x_l) = e^{iOx_l} \sum_{q=1}^n a_q e^{i(y_q - O)x_l} = e^{iOx_l} \mathbf{Y}^c(x_l), \quad x_l \in [-1, 1],$$

where $\mathbf{Y}^c(x_l) = \sum_{q=1}^n a_q e^{i(y_q - O)x}$ is called the centralized local measurement. Note that the relative positions $\tilde{y}_q := y_q - O$'s are located in $[-D, D]$. We can sample \mathbf{Y}^c at $x_l \in [-1, 1]$ with spacing $\frac{\pi}{2D}$ and use the samples to reconstruct \tilde{y}_q 's by the standard MUSIC algorithm. The original source locations can be further recovered as $\hat{y}_1 = \tilde{y}_1 + O, \dots, \hat{y}_n = \tilde{y}_n + O$. We detail these steps in **Algorithm 2** below.

Algorithm 2: MUSIC algorithm with a prior information

- Input:** Noise level σ , local measurements \mathbf{Y} ;
- Input:** Cluster center O , cluster size D ;
- Input:** Spacing of test points TPS ;
- 1: construct the centralized measurement $\mathbf{Y}^c(x_l) = \mathbf{Y}(x_l) e^{-iOx_l}$ with x_l 's spacing by $\frac{\pi}{2D}$;
- 2: Input $[-D, D], TPS, \sigma$, and \mathbf{Y}^c into **Algorithm 1** to recover the relative source locations $\tilde{y}_1, \dots, \tilde{y}_n$;
- 3: Recover the source locations that $\hat{y}_1 = \tilde{y}_1 + O, \dots, \hat{y}_n = \tilde{y}_n + O$;
- Return:** \hat{y}_q 's.
-

We note that for point sources with multi-cluster structure considered in this paper, we can apply the above MUSIC algorithm to each of the local measurements.

3.2 Cluster structure detection

In this section, we develop a subsampled MUSIC algorithm to detect cluster structures. We assume all the point sources are located in a (K, L, D, Ω) -region with $\Omega = 1$. We first choose an sufficiently large interval $[\tilde{O} - \tilde{D}, \tilde{O} + \tilde{D}]$ that covers all the sources. We then choose a proper shrinkage factor $0 < \lambda < 1$, and apply **Algorithm 2** to the global measurement \mathbf{Y} with samples in the interval $[-\lambda, \lambda]$ to get a set of point locations, say c_j , $1 \leq j \leq K'$ for some integer $K' \geq K$. Note that due to subsampling, these locations are not necessarily the locations of the original point sources. However, their presence indicate that there are point sources nearby.

We next estimate the cluster structures. We showed in [21, 22] that n point sources can be resolved if minimum separation distance between them is great than

$$C\pi\left(\frac{\sigma}{m_{\min}}\right)^{\frac{1}{2n-1}}, \quad (3.3)$$

where C is a constant. On the other hand, it is shown numerically that MUSIC algorithm can resolve the point sources under the above condition, see [17]. Therefore, with a shrinkage factor λ the resolution of MUSIC algorithm in the preceding step is of order $O\left(\frac{\pi}{\lambda}\left(\frac{\sigma}{m_{\min}}\right)^{\frac{1}{2n-1}}\right)$. It indicates that when there are two point sources separated greater than $\frac{C\pi}{\lambda}\left(\frac{\sigma}{m_{\min}}\right)^{\frac{1}{3}}$, the MUSIC algorithm will give two peaks. Thus for a peak centered at c_j , the point source/sources that correspond to it should be located in the interval $[c_j - \frac{C\pi}{\lambda}\left(\frac{\sigma}{m_{\min}}\right)^{\frac{1}{3}}, c_j + \frac{C\pi}{\lambda}\left(\frac{\sigma}{m_{\min}}\right)^{\frac{1}{3}}]$. After many numerical experiments, we choose $C = 2$, i.e., the point sources are located in the interval $[c_j - \frac{2\pi}{\lambda}\sigma^{\frac{1}{3}}, c_j + \frac{2\pi}{\lambda}\sigma^{\frac{1}{3}}]$ for $m_{\min} \approx 1$.

We denote $\Gamma_j = [c_j - d, c_j + d]$ with $d = \frac{2\pi}{\lambda\Omega}\sigma^{\frac{1}{3}}$. Notice that there may be multiple c_j 's reconstructed from the subsampled MUSIC algorithm that come from the same cluster. In this case, we may need to combine the involved intervals to get the right cluster structure. For the purpose, we introduce a parameter ICT called the interval combining threshold. We combine the interval Γ_j 's if their centers has distance smaller than ICT . It is clear that ICT should be a proper estimate of the full cluster size $2D$. On the other hand, to ensure that the cluster structure can be recovered successfully, one need the condition that the separation distance between clusters are much larger than their size, i.e. $L \gg D$. We summarize the

cluster structure detection algorithm as **Algorithm 3** below.

Algorithm 3: Cluster structure detection

Input: Noise level σ , Measurement $\mathbf{Y} = (\mathbf{Y}(x_1), \dots, \mathbf{Y}(x_N))$, Shrinkage factor: λ ;

Input: Initial cluster center \tilde{O} , initial cluster size \tilde{D} ;

Input: Spacing of source test points TPS ;

Input: Interval combining threshold ICT ;

1: Construct the subsampled measurement \mathbf{Y}^s by deleting components $Y(x_l)$'s in \mathbf{Y} with $|x_l| > \lambda$;

2: Input $\tilde{O}, \tilde{D}, TPS, \sigma$, and \mathbf{Y}^s into **Algorithm 2** and recover the centers c_j 's;

3: Let $d = \frac{2\pi}{\lambda} \sigma^{\frac{1}{3}}$. If the neighboring c_j 's are separated less than ICT , then the corresponding intervals are combined to form a new interval. After combining all the closely-spaced intervals, we can recover the cluster centers O_j 's as the centers of the new intervals and the cluster sizes D_j 's as the corresponding interval size;

4: Return cluster centers O_j 's, cluster size D_j 's.

We remark that in the above cluster structure detection algorithm, the choice of λ plays an important role. It depends on the cluster structure, the noise level and the available computational power. For large λ , say $\lambda \approx 1$, the underlying cluster structure can be definitely detected. However, it demands high computational cost. On the other hand, for small λ , the cost is reduced, however, the algorithm may not find the cluster structure. In our numerical experiments, we choose $\lambda = \frac{1}{2}$. Note that one can choose a list of shrinkage factors $[\lambda_1, \dots, \lambda_M]$ with $0 < \lambda_1 < \dots < \lambda_M < 1$ and continually detect the cluster structures for each shrinkage factor λ_j until the cluster structure is detected. We leave the question of determining the optimal λ for a future work.

4 Measurement decoupling based super-resolution algorithm

In this section, we develop a fast algorithm for super-resolving point sources with multi-cluster structure. It exploits the ideas of measurement decoupling and is termed D-MUSIC.

For a given set of point sources with multi-cluster structure, say (K, D, L, Ω) , we first detect the cluster structure by **Algorithm 3** with a properly chosen shrinkage factor λ . We then decouple the global measurement into local measurements using the strategy in section 2.2. More precisely, we set $m = 1$ and calculate the multipole number s by (2.8). We then construct the multipole basis $\mathbf{H}^t[j]$'s and recover the multipole coefficients by

$$(\hat{\boldsymbol{\theta}}_1, \dots, \hat{\boldsymbol{\theta}}_K) = \arg \min_{\boldsymbol{\theta}_j, 1 \leq j \leq K} \left\| \sum_{j=1}^K \mathbf{H}^t[j] \boldsymbol{\theta}_j - \mathbf{Y}^t \right\|_2.$$

The measurement decoupling is deemed successful if the residual term $\mathbf{Res}^t = \mathbf{Y}^t - \sum_{j=1}^K \mathbf{H}^t[j] \hat{\boldsymbol{\theta}}_j$ satisfies the condition

$$\|\mathbf{Res}^t\| \leq C_{mea} \sigma$$

for some constant C_{mea} . Here instead of using $\mathbf{H}^t[j] \hat{\boldsymbol{\theta}}_j$'s for the modulated local measurements, we use the following data:

$$\tilde{\mathbf{Y}}_j^t = \mathbf{H}^t[j] \hat{\boldsymbol{\theta}}_j + \mathbf{Res}^t, j = 1, \dots, K.$$

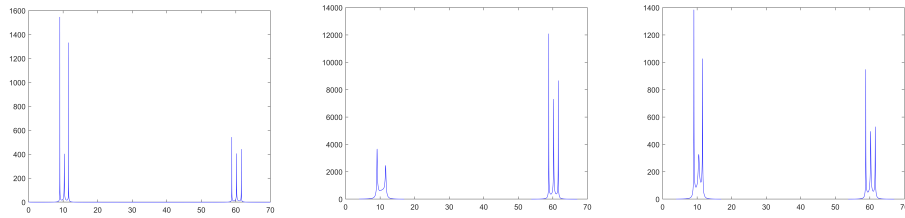
The reason is that numerically $\tilde{\mathbf{Y}}_j^t$ defined above leads to better reconstruction result when was fed to the MUSIC algorithm. See Figure 4.1 for a numerical evidence. It is not clear what is reason behind such an interesting phenomenon. The local measurement can be reconstructed as

$$\tilde{\mathbf{Y}}_j(x_l) = \tilde{\mathbf{Y}}_j^t(x_l)/(1 - x_l^2), \text{ for } x_l \in [-C_{msf}, C_{msf}],$$

where $C_{msf} < 1$ is a cutoff threshold that ensure that $\tilde{\mathbf{Y}}_j(x_l)$ is reconstructed stably. The choice of C_{msf} depends on the noise level and the behavior of the modulation function near the cutoff frequency. We summarize the detail of the measurement decoupling in **Algorithm 4** below.

Algorithm 4: Measurement decoupling by multipole expansion

- Input:** Noise level σ , Measurement $\mathbf{Y} = (\mathbf{Y}(x_1), \dots, \mathbf{Y}(x_N))^T$;
Input: Cluster centers O_1, \dots, O_K , Cluster sizes D_1, \dots, D_K ;
Input: Noise tolerance factor C_{mea} , Measurement modulate function f^t , Measurement cutoff threshold C_{msf} ;
1: Let $D = \max_{j=1}^K (D_j)$, compute the number of multipoles s by $s \geq D, \frac{D^s(s+1)}{s! \sqrt{2s+1}(s+1-d)} \leq \sigma$;
2: Construct the modulated measurement $\mathbf{Y}^t(x_l) = \mathbf{Y}(x_l) f^t(x_l)$, $l = 1, \dots, N$;
3: Construct the corresponding multipole matrix $\mathbf{H}^t[j] = (\mathbf{h}_{0,O_j}^t, \dots, \mathbf{h}_{s-1,O_j}^t)$ by (2.6);
4: Recover $\hat{\boldsymbol{\theta}}_j$'s by $\arg \min_{\boldsymbol{\theta}_j, 1 \leq j \leq K} \|\sum_{j=1}^K \mathbf{H}^t[j] \boldsymbol{\theta}_j - \mathbf{Y}^t\|_2$ and the residual term is $\mathbf{Res}^t = \mathbf{Y}^t - \sum_{j=1}^K \mathbf{H}^t[j] \hat{\boldsymbol{\theta}}_j$;
5: **if** $\frac{1}{\sqrt{N}} \|\sum_{j=1}^K \mathbf{H}^t[j] \hat{\boldsymbol{\theta}}_j - \mathbf{Y}^t\|_2 \leq C_{mea} \sigma$ **then**
 recover modulated local measurements $\tilde{\mathbf{Y}}_j^t = \mathbf{H}^t[j] \hat{\boldsymbol{\theta}}_j + \mathbf{Res}^t$, $j = 1, \dots, K$;
 recover local measurements $\tilde{\mathbf{Y}}_j(x_l) = \tilde{\mathbf{Y}}_j^t(x_l) / f^t(x_l)$, for $x_l \in (-C_{msf}, C_{msf})$;
 Return: measurements $\tilde{\mathbf{Y}}_j$, $j = 1, \dots, K$, DECOUPLE = SUCCESS.
else
 Return: measurement \mathbf{Y} , DECOUPLE = FAIL.
-



(a) MUSIC image from measurement \mathbf{Y} (b) MUSIC image from $\hat{\mathbf{Y}}_j = \mathbf{H}[j] \hat{\boldsymbol{\theta}}_j$ (c) MUSIC image from $\hat{\mathbf{Y}}_j = \mathbf{H}[j] \hat{\boldsymbol{\theta}}_j + \mathbf{Res}$

Figure 4.1: Plots of the MUSIC images of different measurements (no measurements modulation). Figures (a), (b), and (c) are MUSIC images from measurements \mathbf{Y} , $\hat{\mathbf{Y}}_j = \mathbf{H}[j] \hat{\boldsymbol{\theta}}_j$, and $\hat{\mathbf{Y}}_j = \mathbf{H}[j] \hat{\boldsymbol{\theta}}_j + \mathbf{Res}$, respectively. It is shown that three peaks in the left cluster cannot be recovered from the local measurements $\hat{\mathbf{Y}}_j = \mathbf{H}[j] \hat{\boldsymbol{\theta}}_j$, but can be restored from $\hat{\mathbf{Y}}_j = \mathbf{H}[j] \hat{\boldsymbol{\theta}}_j + \mathbf{Res}$.

Finally, we recover the source locations from each local measurement by **Algorithm 2**. We summarize the whole algorithm as **Algorithm 5**.

Algorithm 5: Decoupling based Adaptive MUSIC algorithm (D-MUSIC)

Input: Noise level σ , Measurements: $\mathbf{Y} = (\mathbf{Y}(x_1), \dots, \mathbf{Y}(x_N))^T$, Shrinkage factor: λ ;
Input: Initial guess of the interval containing all sources $[\tilde{O} - \tilde{D}, \tilde{O} + \tilde{D}]$;
Input: Spacing of test points for cluster centers $TPS_{cluster}$, Spacing of test points for point sources TPS_{source} , and Interval combine threshold ICT ;
Input: measurement shrinkage factor C_{msf} ;
1: Initialize the local measurement list as $LML = [\mathbf{Y}]$;
2: Initialize the cluster center list and the cluster size list as $CCL = [\tilde{O}]$, $CSL = [\tilde{D}]$;
3: Input $\sigma, \lambda, \mathbf{Y}, \tilde{O}, \tilde{D}$ and $TPS_{cluster}$ to **Algorithm 3** to recover K cluster centers O_1, \dots, O_K and the cluster sizes D_1, \dots, D_K ;
4: Use **Algorithm 4** to recover the local measurements, $\mathbf{Y}_1, \dots, \mathbf{Y}_K$;
5: **if** $DECOUPLE == SUCCESS$ **then**
 └ Update that $LML = [\mathbf{Y}_1, \dots, \mathbf{Y}_K]$, $CCL = [O_1, \dots, O_K]$, $CSL = [D_1, \dots, D_K]$;
6: Input each local measurement \mathbf{Y}_j , corresponding cluster center O_j , and cluster size D_j in LML, CCL, CSL respectively into **Algorithm 2** to recover all the source locations $\hat{y}_j, j = 1, \dots, n$;
Return: $LOCATIONS = [\hat{y}_1, \dots, \hat{y}_n]$.

We now estimate the computational complexity of **Algorithm 5**. Recall that N is the number of total samples in the measurement. We first consider **Algorithm 3**. Due to subsampling, the number of samples is λN and the computational complexity of SVD therein is of order $O(\lambda^3 N^3)$. In addition, the computational complexity of constructing MUSIC imaging functional is of order $O(N_{cluster} \lambda^2 N^2)$, where $N_{cluster} < N$ is the number of test points for cluster-centers. On the other hand, the computational complexity of **Algorithm 1** therein is $O(\lambda^3 N^3)$ or $O(N_{cluster} \lambda^2 N^2)$. We next consider **Algorithm 4**. Let K be the number of clusters and s be the number of multipole basis for each cluster. Then the size of the multipole matrix in **Algorithm 4** is $sK \times N$. Therefore, the involved computational complexity is of order $O((sK)^2 N)$. Note that $sK \ll N$. Finally, we consider **Algorithm 2**. For each local measurement, let $N_{sub} \ll N$ be the number of samples used for reconstruction. The computational complexity of SVD in the MUSIC algorithm therein is of order $O(N_{sub}^3)$. Let N_{source} be the number of test points for the point sources in the cluster. The computational complexity of constructing the MUSIC imaging functional is of order $O(N_{source} N_{sub}^2)$. Aggregating all these estimates, the computational complexity of **Algorithm 5** is of order

$$O(\lambda^3 N^3 + N_{cluster} \lambda^2 N^2 + (sK)^2 N + KN_{sub}^3 + KN_{source} N_{sub}^2) = O(\lambda^3 N^3 + N_{cluster} \lambda^2 N^2).$$

For comparison, we estimate the computational complexity of the standard MUSIC algorithm (**Algorithm 1**). The computational complexity of SVD therein is of order $O(N^3)$ and of constructing MUSIC imaging functional is of order $O(N_{music} N^2)$, where N_{music} is the number of test points. The computational complexity of standard MUSIC algorithm is of order $O(N^3 + N_{music} N^2)$. Note that $N_{cluster} < N_{music}$ in practice. Therefore the computational complexity of **Algorithm 5** is $\max(\lambda^3, \frac{N_{cluster}}{N_{music}} \lambda^2)$ of that of the standard MUSIC algorithm.

Finally, we conduct numerical experiments for the decoupling based super-resolution algorithm developed above. We demonstrate that its super-resolving ability is comparable to that of the standard MUSIC algorithm but the time cost is substantially lower. We run 1000 experiments with various clusters and reconstruct the source locations by D-MUSIC (**Algorithm 5**) and the standard MUSIC algorithm (**Algorithm 1**) respectively. We set $\Omega = 1$, $\sigma = 10^{-3}$ and the sample number $N = 1000$. We consider (K, L, D, Ω) regions with $L \geq 12\pi$, $D \approx \pi$ and signed measure $\mu = \sum_{j=1}^K \sum_{q=1}^{n_j} a_{q,j} \delta_{y_{q,j}}$ with random cluster number K . We only consider the case where each cluster has no more than three point sources and their separation distance are around 1, which is smaller than the Rayleigh length π . These requirements make sure that the standard MUSIC algorithm can resolve all the point sources. We choose shrinkage factor $\lambda = \frac{1}{2}$ in **Algorithm 5**. The results are shown in Figure 4.2. Figure 4.2 (a) shows that the reconstruction error of the local measurement is of the noise level 10^{-3} , which demonstrates the stability of the measurement decoupling algorithm. Figure 4.2 (b) plots the location recovery of **Algorithm 5** and the standard MUSIC algorithm. It is shown that both algorithms can super-resolving all the point sources and the performances are comparable. Figure 4.2 (c) shows that the new algorithm is ten times faster than the standard MUSIC algorithm.

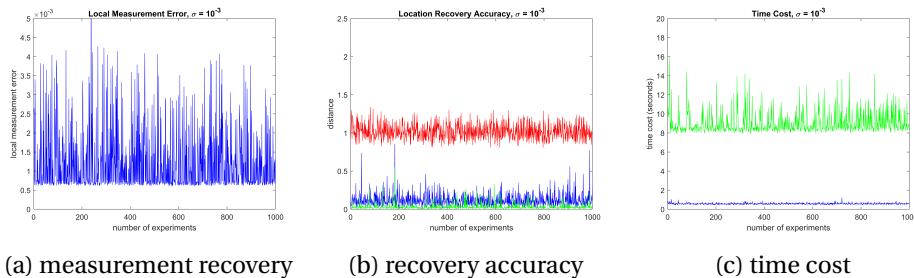


Figure 4.2: Plots of the accuracy of the measurement decoupling, the location recovery, and time cost by **Algorithm 5** and **Algorithm 1**. Figure (a) plots the accuracy of the recovered local measurements by **Algorithm 5**. The blue line shows the maximum recovery error of local measurements in the experiments. The horizontal coordinate is the number of the experiments. Figure (b) plots the location recovery of the two algorithms. The red line (around 1) is the minimal separation distance of underlying point sources in each cluster and the blue line is the maximum deviation of the recovered locations by our algorithm to the ground truth. The green line is the one of the standard MUSIC algorithm. Figure (c) plots the time cost of the two algorithms. The green line is the time cost of the standard MUSIC algorithm and the blue line is the one of our algorithm.

5 Conclusions and future works

In this paper, we proposed an efficient algorithm, termed D-MUSIC, for super-resolving point sources with multi-cluster structure based on a measurement decoupling strategy. We demonstrated that the computational complexity of D-MUSIC is much lower than that of the

standard MUSIC. There remains several interesting issues for future work. The first is on the estimate of the shrinkage factor λ in the cluster structure detection algorithm. The choice of λ plays a important role on the success of the algorithm. The second is on the optimal design of modulation function which can retain frequency components near the cut-off frequency while requiring less stringent condition on the separation distance of clusters for stable decoupling of local measurements. The last one is to extend the algorithm to the more general case when the cluster sizes may have a variety of scales.

6 Appendix

6.1 Proofs of some technical lemma

We denote $\|f\|_{L_\infty((-1,1))} = \max_{x \in [-1,1]} |f(x)|$ and $\|f\|_{L_1((-1,1))} = \int_a^b |f| dx$ for continuous f .

Lemma 6.1. (*Markov brothers' inequality*) *Let $P_n(x)$ be a polynomial of degree at most n , we have*

$$\|P_n^{(k)}(x)\|_{L_\infty((-1,1))} \leq \frac{n^2(n^2-1)\cdots(n^2-(k-1)^2)}{1 \cdot 3 \cdot 5 \cdots (2k-1)} \|P_n(x)\|_{L_\infty((-1,1))}.$$

Lemma 6.2. *Let $P_n(x)$ be a polynomial of degree at most n , we have*

$$\|P_n(x)\|_{L_\infty((-1,1))} \leq (n+1)^2 \|P_n(x)\|_{L_1((-1,1))}.$$

Proof. Given a polynomial p of degree at most n , consider $q(x) = \int_{-1}^x p(t) dt$. We have $|q(x)| \leq \int_{-1}^x |p(t)| dt \leq \|p\|_{L_1((-1,1))}$ and therefore $\|q\|_{L_\infty((-1,1))} \leq \|p\|_{L_1((-1,1))}$. By Lemma 6.1, one has $\|q'\|_{L_\infty((-1,1))} \leq (n+1)^2 \|q\|_{L_\infty((-1,1))}$ since q is of degree at most $n+1$. By $q' = p$, we have

$$\|p\|_{L_\infty((-1,1))} \leq (n+1)^2 \|p\|_{L_1((-1,1))}.$$

□

Lemma 6.3. *Let ψ be a polynomial of degree at most n , then for $\lambda \geq 2n^2$ we have*

$$\left| \int_{-1}^1 e^{i\lambda x} \psi(x) dx \right| < \frac{3.2 \|\psi\|_{L_\infty((-1,1))}}{\lambda}.$$

Suppose further that $\psi(\pm 1) = 0, \psi'(\pm 1) = 0$, we have

$$\left| \int_{-1}^1 e^{i\lambda x} \psi(x) dx \right| < \frac{0.8n^4 \|\psi\|_{L_\infty((-1,1))}}{\lambda^3}.$$

Proof. By integration by parts, we have

$$\int_{-1}^1 e^{i\lambda x} \psi(x) dx = \frac{e^{i\lambda x} \psi(x)}{i\lambda} \Big|_{-1}^1 - \frac{\int_{-1}^1 e^{i\lambda x} \psi'(x) dx}{i\lambda} = \frac{1}{i\lambda} \sum_{k=0}^n \frac{e^{i\lambda x} \psi^{(k)}(x)}{(-i\lambda)^k} \Big|_{-1}^1.$$

Taking absolute value to both sides, we have

$$\begin{aligned}
\left| \int_{-1}^1 e^{i\lambda x} \psi(x) dx \right| &\leq \frac{1}{\lambda} \left(2 \sum_{k=0}^n \frac{\|\psi^{(k)}\|_{L_\infty([-1,1])}}{\lambda^k} \right) \\
&\leq \frac{2\|\psi\|_{L_\infty([-1,1])}}{\lambda} \left(1 + \frac{n^2}{\lambda} + \frac{n^2(n^2-1)}{3\lambda^2} + \dots + \frac{n^2(n^2-1)\cdots(n^2-(n-1)^2)}{(2n-1)!!\lambda^n} \right) \quad (\text{by Lemma 6.1}) \\
&< \frac{3.2\|\psi\|_{L_\infty([-1,1])}}{\lambda}. \quad (\text{by } \lambda \geq 2n^2)
\end{aligned}$$

Moreover, when $\psi(\pm 1) = 0, \psi'(\pm 1) = 0$,

$$\int_{-1}^1 e^{i\lambda x} \psi(x) dx = \frac{1}{i\lambda} \sum_{k=2}^n \frac{e^{i\lambda x} \psi^{(k)}(x)}{(-i\lambda)^k} \Big|_{-1}^1.$$

Taking absolute value to both sides, we have

$$\begin{aligned}
\left| \int_{-1}^1 e^{i\lambda x} \psi(x) dx \right| &\leq \frac{1}{\lambda} \left(2 \sum_{k=2}^n \frac{\|\psi^{(k)}\|_{L_\infty([-1,1])}}{\lambda^k} \right) \\
&\leq \frac{2\|\psi\|_{L_\infty([-1,1])}}{\lambda} \left(\frac{n^2(n^2-1)}{3\lambda^2} + \dots + \frac{n^2(n^2-1)\cdots(n^2-(n-1)^2)}{(2n-1)!!\lambda^n} \right) \quad (\text{by Lemma 6.1}) \\
&< \frac{0.8n^4\|\psi\|_{L_\infty([-1,1])}}{\lambda^3}, \quad (\text{by } \lambda \geq 2n^2)
\end{aligned}$$

whence the lemma follows. □

6.2 A peak selection algorithm

Algorithm 6: Peak selection algorithm

Input: Image $IMG = (f(\omega_1), \dots, f(\omega_M))$;

Input: Peak compare range PCR , differential compare range DCR , differential compare threshold DCT ;

1: Initialize the Local maximum points $LMP = []$, peak points $PP = []$;

2: Differentiate the image IMG to get the $DIMG = (f'(\omega_1), \dots, f'(\omega_M))$;

3: **for** $j = 1 : M$ **do**

if $f(\omega_j) = \max(f(\omega_{j-PCR}), f(\omega_{j-PCR+1}), \dots, f(\omega_{j+PCR}))$ **then**

 LMP appends ω_j ;

4: **for** ω_j *in* LMP **do**

if $\max(|f'(\omega_{j-DCR})|, |f'(\omega_{j-DCR+1})|, \dots, |f'(\omega_{j+DCR})|) \geq DCT$ **then**

 PP appends ω_j ;

Return: PP .

References

- [1] Dmitry Batenkov, Benedikt Diederichs, Gil Goldman, and Yosef Yomdin. The spectral properties of vandermonde matrices with clustered nodes. *Linear Algebra and its Applications*, 609:37–72, 2021.
- [2] Dmitry Batenkov, Gil Goldman, and Yosef Yomdin. Super-resolution of near-colliding point sources. *Information and Inference: A Journal of the IMA*, 05 2020. iaaa005.
- [3] Brett Bernstein and Carlos Fernandez-Granda. Deconvolution of point sources: a sampling theorem and robustness guarantees. *Communications on Pure and Applied Mathematics*, 72(6):1152–1230, 2019.
- [4] Jian-Feng Cai, Tianming Wang, and Ke Wei. Fast and provable algorithms for spectrally sparse signal reconstruction via low-rank hankel matrix completion. *Applied and Computational Harmonic Analysis*, 46(1):94–121, 2019.
- [5] Emmanuel J. Candès and Carlos Fernandez-Granda. Super-resolution from noisy data. *Journal of Fourier Analysis and Applications*, 19(6):1229–1254, 2013.
- [6] Emmanuel J. Candès and Carlos Fernandez-Granda. Towards a mathematical theory of super-resolution. *Communications on Pure and Applied Mathematics*, 67(6):906–956, 2014.
- [7] Yuejie Chi and Maxime Ferreira Da Costa. Harnessing sparsity over the continuum: Atomic norm minimization for superresolution. *IEEE Signal Processing Magazine*, 37(2):39–57, 2020.
- [8] Quentin Denoyelle, Vincent Duval, and Gabriel Peyré. Support recovery for sparse super-resolution of positive measures. *Journal of Fourier Analysis and Applications*, 23(5):1153–1194, 2017.
- [9] Vincent Duval and Gabriel Peyré. Exact support recovery for sparse spikes deconvolution. *Foundations of Computational Mathematics*, 15(5):1315–1355, 2015.
- [10] Yonina C Eldar, Patrick Kuppinger, and Helmut Bolcskei. Block-sparse signals: Uncertainty relations and efficient recovery. *IEEE Transactions on Signal Processing*, 58(6):3042–3054, 2010.
- [11] Yonina C Eldar and Moshe Mishali. Block sparsity and sampling over a union of subspaces. In *2009 16th International Conference on Digital Signal Processing*, pages 1–8. IEEE, 2009.
- [12] Yonina C Eldar and Moshe Mishali. Robust recovery of signals from a structured union of subspaces. *IEEE Transactions on Information Theory*, 55(11):5302–5316, 2009.
- [13] Carlos Fernandez-Granda. Support detection in super-resolution. In *Proceedings of the 10th International Conference on Sampling Theory and Applications (SampTA 2013)*, pages 145–148, 2013.

- [14] Keyong Han and Arye Nehorai. Improved source number detection and direction estimation with nested arrays and ulas using jackknifing. *IEEE Transactions on Signal Processing*, 61(23):6118–6128, 2013.
- [15] Zhaoshui He, Andrzej Cichocki, Shengli Xie, and Kyuwan Choi. Detecting the number of clusters in n-way probabilistic clustering. *IEEE Transactions on Pattern Analysis and Machine Intelligence*, 32(11):2006–2021, 2010.
- [16] Yingbo Hua and Tapan K. Sarkar. Matrix pencil method for estimating parameters of exponentially damped/undamped sinusoids in noise. *IEEE Transactions on Acoustics, Speech, and Signal Processing*, 38(5):814–824, 1990.
- [17] Weilin Li and Wenjing Liao. Stable super-resolution limit and smallest singular value of restricted fourier matrices. *Applied and Computational Harmonic Analysis*, 51:118–156, 2021.
- [18] Weilin Li, Wenjing Liao, and Albert Fannjiang. Super-resolution limit of the esprit algorithm. *IEEE Transactions on Information Theory*, 66(7):4593–4608.
- [19] Wenjing Liao and Albert C. Fannjiang. Music for single-snapshot spectral estimation: Stability and super-resolution. *Applied and Computational Harmonic Analysis*, 40(1):33–67, 2016.
- [20] Ping Liu and Hai Zhang. A mathematical theory of computational resolution limit in multi-dimensional spaces. *Inverse Problems*, 37(10):104001, 2021.
- [21] Ping Liu and Hai Zhang. A theory of computational resolution limit for line spectral estimation. *IEEE Transactions on Information Theory*, 67(7):4812–4827, 2021.
- [22] Ping Liu and Hai Zhang. A mathematical theory of the computational resolution limit in one dimension. *Applied and Computational Harmonic Analysis*, 56:402–446, 2022.
- [23] Veniamin I Morgenshtern. Super-resolution of positive sources on an arbitrarily fine grid. *arXiv preprint arXiv:2005.06756*, 2020.
- [24] Veniamin I. Morgenshtern and Emmanuel J. Candes. Super-resolution of positive sources: The discrete setup. *SIAM Journal on Imaging Sciences*, 9(1):412–444, 2016.
- [25] Richard Roy and Thomas Kailath. Esprit-estimation of signal parameters via rotational invariance techniques. *IEEE Transactions on acoustics, speech, and signal processing*, 37(7):984–995, 1989.
- [26] Ralph Schmidt. Multiple emitter location and signal parameter estimation. *IEEE transactions on antennas and propagation*, 34(3):276–280, 1986.
- [27] Mihailo Stojnic, Farzad Parvaresh, and Babak Hassibi. On the reconstruction of block-sparse signals with an optimal number of measurements. *IEEE Transactions on Signal Processing*, 57(8):3075–3085, 2009.

- [28] Gongguo Tang. Resolution limits for atomic decompositions via markov-bernstein type inequalities. In *2015 International Conference on Sampling Theory and Applications (SampTA)*, pages 548–552. IEEE, 2015.
- [29] Gongguo Tang, Badri Narayan Bhaskar, and Benjamin Recht. Near minimax line spectral estimation. *IEEE Transactions on Information Theory*, 61(1):499–512, 2014.
- [30] Yung-Yi Wang, Liang-Cheng Lee, Shih-Jen Yang, and Jiunn-Tsair Chen. A tree structure one-dimensional based algorithm for estimating the two-dimensional direction of arrivals and its performance analysis. *IEEE transactions on antennas and propagation*, 56(1):178–188, 2008.
- [31] Mati Wax and Thomas Kailath. Detection of signals by information theoretic criteria. *IEEE Transactions on acoustics, speech, and signal processing*, 33(2):387–392, 1985.